Positive- and negative-ion formation in low-energy O^+-Cu(001) scattering

C. A. Keller, A. C. Lavery, and B. H. Cooper
Laboratory of Atomic and Solid State Physics, Cornell University, Ithaca, New York 14853-2501
(Received 17 November 1997; revised manuscript received 29 May 1998)

For incident 0.4–7-keV O^+ beams scattered from Cu(001), we have measured energy and angular distributions of O^+ and O^- ions in the scattered flux, and performed accurate quantitative measurements of the O^+/O^- ratios. The O^+/O^- ratios depend on the scattering geometry and, for a given geometry, decrease with decreasing scattered perpendicular velocity. The qualitative differences between the energy and angular spectra for the scattered positive and negative ions indicate that this trend is due to the rapid decrease of the O^+ fraction. These data and general arguments based on the energies of the states of the O-Cu system are used to identify key mechanisms responsible for the presence of O^+ and O^- in the scattered flux. We conclude that the resonant and Auger charge transfer mechanisms are both important. Furthermore, the data indicate that the O^+ ions are generated in the hard collision between the incident atom and a surface atom. These collisions explain the geometry dependence of the measured O^+/O^- ratios. [S0163-1829(98)00640-7]

I. INTRODUCTION

Charge exchange is a fundamental process that occurs in dynamical interactions of atoms or molecules with surfaces, and plays a central role in processes such as dissociative chemisorption, laser-induced desorption, and the formation and deexcitation of excited states. Scattering experiments in which final charge-state distributions of the scattered particles are measured provide a powerful means of investigating electron-transfer mechanisms. By varying parameters such as the incident beam energy and scattering geometry, the dependence of different charge-exchange mechanisms on the various time and energy scales can be determined. The goal of such experiments is to provide a better understanding of nonadiabatic electronic interactions of atoms with surfaces.

Although charge exchange between surfaces and reactive species, such as oxygen, has been the focus of several recent investigations,[1–5] a thorough understanding has not yet been achieved. For a recent review see Niehus *et al.*[1] and references therein. While there are both fundamental and practical reasons to improve our understanding of these systems, developing this understanding is an experimental and theoretical challenge due to the large number of effects that must be considered. The effects we consider are the resonant[6] and Auger[7–9] charge-exchange mechanisms, electron promotion in hard collisions,[10–14] relaxation of the scattered excited states through Auger autoionization,[10,11,13] coupling to collision dynamics,[15] and the velocity of the scattering atom relative to the surface electrons.[16,17] Furthermore, the intrinsic multichannel character of the problem due to the degenerate *p* orbital electrons[18] has to be considered. Applications involving charge transfer in energetic oxygen collisions with metal surfaces include plasma processing and etching of surfaces, oxide formation, secondary ion mass spectrometry, and satellite interactions with the atmosphere in low earth orbit.

Recent studies of charge transfer using oxygen beams have involved scattering at grazing angles from metals,[2] insulators,[19] and semiconductors.[4] At grazing angles, the interaction of the incident ion with the surface takes place over many lattice sites. Some of these studies have involved scattering of highly charged oxygen ions.[2] Here, for scattering of 0.4–7-keV O^+ from Cu(001) at angles far from grazing, we present energy- and angle-resolved measurements of the distributions of the scattered positive and negative ions. Trajectory analysis is used to correlate well-defined trajectory types with features in the measured distributions. Access to a wide range of scattering angles enables us to choose scattering geometries where single scattering trajectories are easily distinguished from the background of multiple scattering trajectories. The ability to identify and isolate specific trajectory types has been used to study charge exchange mechanisms in the scattering of noble gas[11] or alkali atoms[10,15] and has proven indispensable in identifying the charge-transfer mechanisms for the O-Cu system. The only other charge-transfer experiments we are aware of where keV oxygen leaves a metal surface at angles far from grazing are some recent studies involving scattering from polycrystalline samples,[5] and experiments in which O atoms adsorbed on a surface are scattered from that surface by direct recoil collisions with keV noble gas ions.[20] In the latter experiments, the O atoms necessarily interact with an adsorbate-covered surface, which complicates the analysis.

Our goal in this paper is to identify the key mechanisms responsible for the presence of O^+ and O^- in the outgoing flux. The data and general physical arguments based on the energies of the states of the oxygen-copper system indicate that both resonant and Auger charge transfer must occur to explain the observed O^+ to O^- ratios. The measurements also indicate that the O^+ ions observed in the scattered flux are generated in hard collisions between the incident O atoms and the Cu surface atoms.

In Sec. II, we present our experimental apparatus and measurement techniques. In Sec. III we present experimental results for scattering of 0.4–7-keV O^+ from Cu(001). These include measured positive to negative ion ratios as a function of outgoing velocity and scattering geometry for scattered ions that have undergone quasisingle[21] (QS) -type collisions with the surface, scattered positive- and negative-ion distri-

butions for a wide range of incident energies and scattering angles, and a measurement of the scattered ion and neutral fractions for a single incident energy. In Sec. IV we introduce a general framework within which to examine charge transfer for the O-Cu system and discuss what our results indicate about the charge-transfer mechanisms. In Sec. V we briefly summarize our results.

II. EXPERIMENTAL APPARATUS AND TECHNIQUE

The experimental apparatus consists of a low- and hyperthermal-energy beamline and UHV scattering chamber. The ion source[22] uses electrons from a resistively heated thoriated-iridium filament to produce ions from almost any introduced gas. Positive ions extracted from the source are accelerated, mass-selected, and monochromated before reaching the scattering chamber. A source gas mixture of 15% O_2 and 85% Ne was chosen to provide high O^+ yields and to minimize the partial pressure of background O_2 in the scattering chamber. The source electronics actively stabilize the filament emission current—by adjusting the filament heating current—to reduce instabilities associated with operating a hot filament in an oxygen atmosphere. The source and beamline produce stable, well-collimated, monoenergetic ion beams[23] focused into a 1-mm (full width at half maximum) spot with energies ranging from 100 eV to 7 keV, and corresponding currents of 1–50 nA.

The upper tier of our vacuum chamber is for sample preparation and analysis; the lower tier is for scattering and houses a neutral particle detector (NPD)—part of a time-of-flight (TOF) system—and a hemispherical electrostatic analyzer (ESA). Both detectors can be rotated about the sample to access different scattering angles. The ESA and its entrance optics provide energy (1.6% of the pass energy) and angular (1° full width) resolution of the scattered particles. A channel electron multiplier[24] (CEM) at the exit of the ESA serves as our detector. Further details of the NPD and TOF system are given elsewhere.[25] A sample manipulator with six degrees of freedom moves the sample between the upper and lower tiers of the chamber, allows accurate alignment for scattering, and provides access to a large range of scattering geometries. More detailed discussions of the ion scattering apparatus and alignment procedure are also given elsewhere.[26,27]

Since charge-transfer measurements are very sensitive to low levels of surface contamination, care was taken to monitor impurities on the crystal surface. Samples were cleaned by repeated sputter and anneal cycles. After the first cleaning of a new crystal, cleanliness was verified by depositing a Cs overlayer, annealing to 200 °C, and then using Auger electron spectroscopy (AES) to look for contaminants. This procedure brings impurities to the surface and provides a more stringent test for contamination near the surface than AES measurements on a freshly sputtered and annealed surface. The sample was cleaned before each measurement by annealing briefly at 600 °C, sputtering with 500-eV Ar^+ incident at 80 °C from the surface normal, and again annealing briefly at 600 °C. AES measurements have shown that the first anneal cycle causes oxygen buried during scattering to segregate to the surface where it can be sputtered off. The second anneal removes residual Ar in addition to annealing surface defects created during sputtering. Low-energy electron diffraction was used to monitor surface order. At the start of each scattering measurement the sample was well ordered and clean to within the sensitivity limits of AES.

To ensure that dosing due to the incident beam did not affect our scattered ion fractions, we measured the intensity of the QS peaks for both positive and negative scattered ions as a function of beam dose. With the beam incident on the sample at 45° from the surface normal, the intensity of scattered O^- changed by as much as 13%, and that of O^+ by 5%, before saturating. For the quantitative measurements of the scattered positive- to negative-ion ratio presented in this paper, these effects were kept below 1.5% by limiting the current on sample to ~ 1 nA.[28] Successive spectra taken without cleaning the sample between measurements were identical; this indicates that the effects on the data from dosing by the incident beam and adsorption of residual gases were negligible. The base pressure of the UHV chamber was 6×10^{-11} Torr and the working pressure, with the beam running, was 2×10^{-10} Torr.

Careful design of the CEM input optics used for ion detection optimizes the quantitative measurement capabilities of the CEM for both positive and negative ions, and prevents the detection of stray electrons. The CEM was calibrated as a function of both energy and ion charge. These calibrations showed that the efficiencies of the CEM for detecting positive and negative oxygen ions were not identical and were not equal to one. The calibration also showed that optics that ensure secondary electron collection at the entrance of the CEM are required for accurate quantitative measurement of both positive and negative ions. The detection system and calibration are explained in detail in Ref. 29. All of the quantitative data presented in this paper have been normalized for the transmission function of the ESA, the efficiency of the CEM, and the incident-beam dose.

Throughout this paper all measurements are done in the scattering plane. Both the incident angle θ_i and the final angle θ_f are measured from the surface normal, as shown in Fig. 1. The incident angle is always positive, and a positive final angle represents scattering on the side of the surface normal away from the incident beam. For example, $\theta_i=\theta_f=45°$ corresponds to specular forward scattering, and $\theta_i=-\theta_f=45°$ to direct backscattering.

III. MEASUREMENTS

A. Positive- to negative-ion ratios and scattered ion fractions

By coupling trajectory analysis with careful selection of scattering geometries, it is possible to determine scattered ion intensities for a single well-defined trajectory (collision) type. In this paper, we have chosen to focus on QS trajectories that scatter from the first layer of atoms on the surface. These are kinematically the simplest trajectories, as well as being the only trajectory type that is easily isolated from the background at keV scattering energies.[30] The incident angle and crystal azimuth have been chosen such that the first layer of atoms on the surface shadows the deeper layers. Thus, even at higher incident energies, the second and deeper layers do not contribute to the QS scattering.[31]

As will be discussed in Sec. III C, the separation of the QS peak from the background due to other types of scatter-

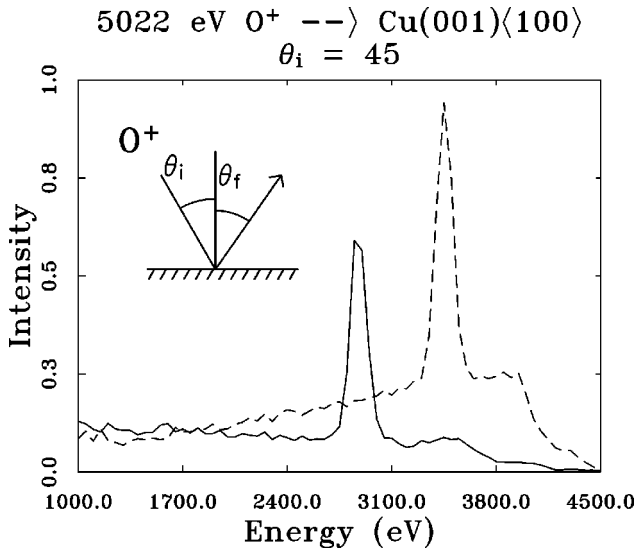

FIG. 1. Negative-ion spectra for 5022-eV O^+ incident on Cu(001)⟨100⟩ $\theta_i=45°$. Data are shown for $\theta_f=65°$, dashed line, and $\theta_f=45°$, solid line. These spectra show the separability of the background and the QS peak at these geometries. The inset shows the in-plane scattering geometry used throughout this paper, where θ_i and θ_f are the incident and final angles, respectively.

ing trajectories is often complicated by the highly peaked shape of the background. However, careful choice of the scattering geometry can make the separation much easier. Figure 1 shows negative-ion spectra, which generally have a much larger background than the positive-ion spectra, for 5022-eV O^+ incident along the ⟨100⟩ azimuth with an incident angle of 45° and final angles of 45° and 65°. These geometries, where the QS peak is easily separated from the background, were used for the measurement of the positive to negative-ion ratios.

For these two scattering geometries ($\theta_i=\theta_f=45°$ and $\theta_i=45°$, $\theta_f=65°$), Fig. 2 shows the ratio of the measured positive and negative QS peak intensities as a function of the inverse perpendicular velocity[32] of the scattered particles. For the $\theta_i=\theta_f=45°$ geometry, the positive- to negative-ion ratio was measured for incident energies ranging from 2 to 7 keV, and for the $\theta_i=45°, \theta_f=65°$ geometry, it was measured for 2.5–7 keV. Measurements were performed at lower incident energies, but the very low yield of positive ions made the analysis unreliable. For each scattering geometry and each incident energy, the data analysis consisted of correcting the positive and negative scattered ion spectra for the transmission function of the ESA, the CEM efficiency, and the beam intensity, performing the separation of each QS peak from the background, and taking the ratio of the integrated intensity of the QS peak of the positive ions to that of the negative ions. The integrated intensity of the QS peak is calculated by fitting a spectrum with a Gaussian plus a linear background and integrating the area under the Gaussian. The data show that the ratio of positive to negative ions in the scattered flux drops dramatically with decreasing final perpendicular velocity. Note that, for a given perpendicular velocity, the ratio depends on the scattering geometry. This indicates that either collisional processes or the velocity of the atom relative to the electrons in the surface influence the final charge state.

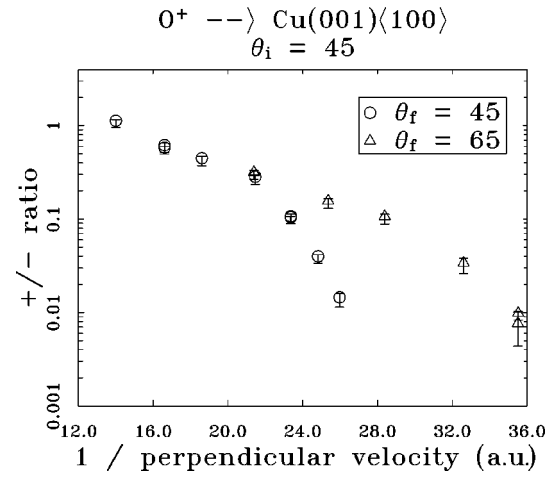

FIG. 2. Ratio of positive to negative scattered ions for O^+ incident on Cu(001)⟨100⟩ $\theta_i=45°$. The circles are for $\theta_f=45°$, and, from left to right, $E_i=7$, 5, 4, 3, 2.5, 2.2, and 2 keV, where E_i is the incident energy. The triangles are for $\theta_f=65°$, and, from left to right $E_i=7$, 5, 4, 3, and 2.5 keV. The perpendicular velocity is given in atomic units, 1 a.u.$=2.2\times10^8$ cm/s.

To determine what fraction of the scattered particles are ions, measurements of the total (positive plus negative) ion fraction are needed. Using the neutral particle detector and time-of-flight system, we have made a preliminary measurement of the total ion fraction for 1-keV O^+ incident along the ⟨100⟩ azimuth of Cu(001), with $\theta_i=\theta_f=45°$ (the scattered perpendicular velocity is 0.027 a.u.). We have found that ions comprise approximately 10% of the scattered flux at this energy. The positive- to negative-ion ratio measurement (see Fig. 2) indicates that this is almost entirely negative ions. Modifications of the NPD and TOF system are being made to extend the ion fraction measurements to higher incident energies.

B. Angular spectra of the quasisingle trajectory type

For 0.4–5-keV O^+ ion beams incident along the ⟨100⟩ azimuth of the Cu(001) surface at 45° from the surface normal, we have measured energy spectra for scattered positive and negative ions over a large range of final angles θ_f. These sets of spectra revealed a number of interesting trends in the positive- and negative-ion yields and provided the information needed to select optimal geometries for the quantitative measurement of the positive- to negative-ion ratio.

Figure 3 shows the integrated intensity of the QS peak plotted as a function of the final scattering angle θ_f. A decrease in the incident energy or an increase in the final angle corresponds to a decrease both in the final perpendicular velocity of the scattered atom and in the energy transferred from the incident ion to the surface atom in the QS collision. Again, the incident angle and crystal azimuth have been chosen such that the second and deeper layers do not contribute to the QS scattering due to shadowing by the first layer.

The shape of each angular spectrum depends on two factors, the charge exchange near the surface, and the kinematics of the scattering. At the top of Fig. 3, we have included an angular spectrum for the integrated intensity of the 400-eV QS peaks of Na^+ scattered from Cu(001). Previous

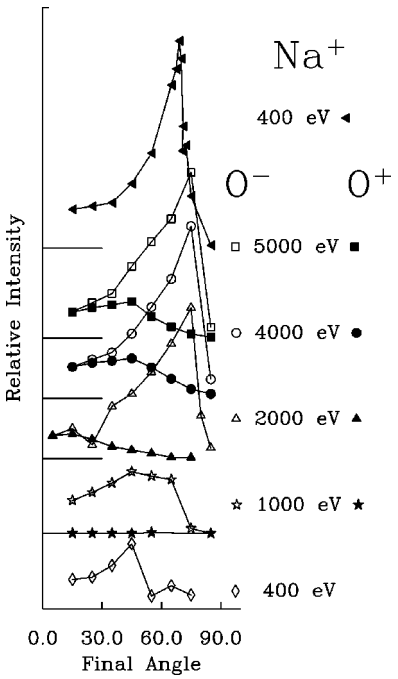

FIG. 3. Trends in low-energy O^+ scattering. Each curve is determined from a set of energy spectra for O^+ incident on Cu(001)⟨100⟩ with $\theta_i = 45°$ and θ_f between 15° and 85°. Each point is the integrated intensity of the QS peak plotted as a function of the final angle at which the QS peak was measured. The open symbols are scattered negative ions, and the filled symbols are scattered positive ions. The solid lines are to guide the eye. The curves are all (except the 1000-eV positive-ion curve where the peaks are extremely small) scaled to the intensity of the 5000-eV negative-ion spectrum at $\theta_f = 15°$. From left to right in each curve the θ_f values are as follows. The Na^+ data at 400 eV are included for comparison (see text).

Energy (eV)	Ion charge	Final angles
5000	−	15,25,35,45,55,65,75,85
5000	+	15,25,35,45,55,65,75,85
4000	−	15,25,35,45,55,65,75,85
4000	+	15,25,35,45,55,65,75,85
2000	−	5,15,25,35,45,55,65,75,80,85
2000	+	5,15,25,35,45,55,65,75
1000	−	15,25,35,45,55,65,75,85
1000	+	15,25,35,45,55,85
400	−	15,25,35,45,55,65,75
400	+	no signal above noise

work[16] has demonstrated that charge exchange has a negligible effect on the shape of the Na^+ angular spectrum. That is, the ion survival probability is constant across the velocity range of the scattered particles. This means that the shape of the Na^+ curve is determined almost entirely by the kinematics of the scattering. In the Na^+ spectrum of Fig. 3, the prominent peak is a kinematic rainbow[30] caused by the periodic nature of the scattering potential. We use the shape of the Na^+ curve as a reference in the following discussion. It can be seen that the O^- curves at 2000, 4000, and 5000 eV have the same general shape as the Na^+ data. Thus, for these O^- spectra the behavior is also predominantly kinematic. This implies that the probability of scattering as an O^- is relatively constant over the range of final angles and incident energies of these measurements. However, at 1000 eV and below, the shape of the negative-ion angular spectrum deviates from a purely kinematically determined shape, indicating that the negative-ion fraction decreases at larger final angles.

The angular spectra of the positive ions shown in Fig. 3 are very different from both the negative-ion spectra and the 400-eV Na^+ reference data. Even at the highest incident energies, the shapes of the positive-ion spectra indicate that the positive-ion fraction changes rapidly with final angle. When the incident energy is reduced to 1000 eV, the scattered positive-ion intensity has effectively disappeared.

Some interesting trends are evident from the shapes of the spectra shown in Fig. 3: (1) at lower collision energies (incident energies of 1000 eV and below) and perpendicular velocities both the positive- and negative-ion fractions decrease; (2) at higher collision energies (2000 eV and above) the positive-ion fraction decreases rapidly with increasing final angle (decreasing perpendicular velocity) while the negative-ion fraction remains relatively constant. We will use this information in Sec. IV.

C. Charge exchange in surface vs subsurface scattering—a detailed analysis of the background of the QS peak

We can also make use of scattered-energy spectra to learn about charge-transfer mechanisms for different trajectory-types. There is typically a larger background under the QS peak in the negative-ion spectra than in the positive-ion spectra. This can be seen clearly in Fig. 4(a) for 5011-eV O^+ incident along the ⟨100⟩ azimuth with $\theta_i = 65°$ and $\theta_f = -10°$ (total scattering angle=125°), where the narrow QS peak appears on top of a broad wedge-shaped background. In these spectra, chosen because of the particularly dramatic difference in the background intensities, the positive and negative QS single peaks have approximately the same magnitudes, but the intensity of the background in the negative-ion spectrum is much larger than that in the positive-ion spectrum. This geometry also illustrates the difficulties involved in separating the QS peak from the background. Figure 5 shows a similar set of energy spectra taken with $\theta_i = 45°$ and $\theta_f = 65°$; this is one of the geometries used in the quantitative measurement of the positive- to negative-ion ratio (Fig. 2). Here too, it can be seen that there is a much larger background under the QS peak in the negative-ion spectrum than in the positive-ion spectrum.

To understand these differences in background intensities, we have used the classical trajectory simulation code SAFARI (Ref. 33) with a Ziegler-Biersack-Littmark (ZBL) (O-Cu) potential[34] to classify the trajectories that contribute to these spectra. Figures 4(a) and 5(a) show SAFARI simulations for comparison to the data. The simulations reproduce the broad wedge-shaped background and the narrow QS peak of the measured spectra, but fail to accurately reproduce the energies of the peaks. The discrepancy in the energies can be attributed to inelastic losses resulting from electronic excitations[12] that are not included in the simulation. Figures 4(b) and 5(b) show separate calculated spectra for scattering from the first-layer atoms of the crystal and from deeper layers. From these simulations, it is clear that the background

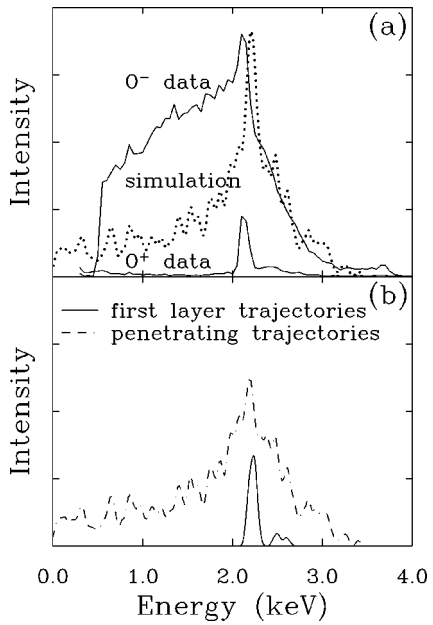

FIG. 4. (a) Positive and negative measured ion spectra (solid lines) and a kinematic simulation (dotted line) for 5011-eV (5000 eV in simulation) O^+ incident on Cu(001)⟨100⟩ $\theta_i = 65°$, $\theta_f = -10°$. Note the similar magnitude of the QS peak in each spectrum and the large difference in the magnitudes of the backgrounds. Perpendicular velocity for QS peak is 0.072 a.u. (b) Breakdown of simulation into trajectories scattering from the first layer and those scattering from deeper layers showing that the background is due to scattering from deeper layers.

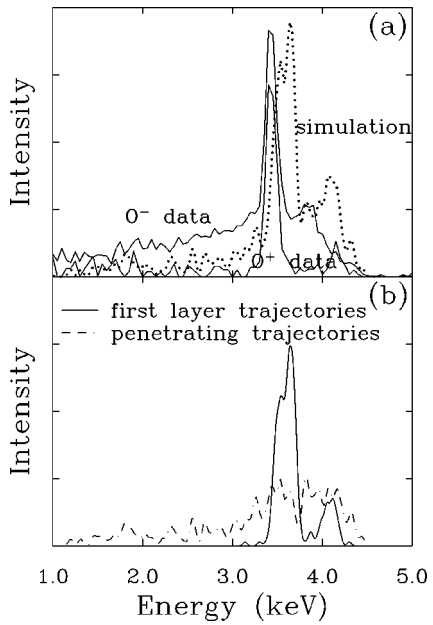

FIG. 5. Modeling of background for 5-keV O^+ incident on Cu(001)⟨100⟩ $\theta_i = 45°$, $\theta_f = 65°$. Incident energy is 5000 eV in the model and 5022 eV in the data. (a) Comparison of model with measured O^- and O^+ spectra. The spectra are scaled to give equal QS peak heights. (b) Breakdown of simulation into trajectories scattering from the first layer and those scattering from deeper layers showing that the background is due to scattering from deeper layers.

in the measured spectra results from trajectories that penetrate through the first layer of Cu atoms. An exception to this occurs at energies just above the QS peak where the quasidouble (trajectories involving collisions with two surface atoms, both lying in the scattering plane) peak gives the background its characteristic wedge shape. This is particularly clear in Fig. 5 where the QS trajectories give the larger peak at 3600 eV and quasidouble trajectories give the smaller peak at 4100 eV.

Since at keV incident energies the scattering potential depends only weakly on the atom's charge state, the scattered energy distribution of all particles (neutrals and ions) is determined almost entirely by the scattering kinematics. Consequently, the large difference in the background intensities of the positive and negative spectra of Fig. 4, and the similar intensities of the QS peaks, show that the background has a charge state distribution different from that of the QS peak. This is particularly interesting when considering the background intensities at energies just below the QS peak. This part of the background contains trajectories with final velocities nearly identical to those of the QS trajectories and yet with a dramatically different charge-state distribution. This will be discussed further in the next section.

IV. DISCUSSION

We have seen from the data presented in the previous section that both positive and negative ions are formed during scattering of O^+ from Cu(001), and that the energy spectra and angular distributions are qualitatively different for the scattered positive and negative ions. Since our objective is to identify the mechanisms responsible for the presence of positive and negative ions in the scattered flux, we begin this section by developing a general framework for discussing charge exchange in the O-Cu system. In Sec. IV A, we draw some general qualitative conclusions about the resonant and Auger charge-exchange mechanisms for this system, and we draw our main conclusions in Secs. IV B and IV C when we examine the data in detail.

A. General

Charge transfer for the oxygen-metal system is often discussed in the language of atomic ionization (I) and affinity (A) levels and their energies relative to the Fermi level of the metal[5,9,18] (see Fig. 6). Each ionization or affinity level corresponds to a pair of states between which a transition can be made by transferring an electron between the atom and the metal. As an O atom is brought closer to the surface, the image potential causes the energy of the ionization (affinity) level to shift upwards (downwards) and hybridization of the atomic and metallic states causes the level to broaden into a resonance. To account for the scattered oxygen species that we observe, we include the seven allowed states from the neutral oxygen ($2p^4$), positive-ion ($2p^3$), and negative-ion ($2p^5$) configurations, as shown in Fig. 7. These include (i) the neutral atom ground state $O(^3P)$ and two metastable excited states $O(^1D)$ and $O(^1S)$, (ii) the positive-ion ground state $O^+(^4S)$ and two excited states $O^+(^2D)$ and $O^+(^2P)$, and (iii) the negative-ion $O^-(^2P)$ state. Unlike a system that can be described by a single level, charge transfer in a multistate system is not determined simply by whether an individual affinity or ionization level is above or below the

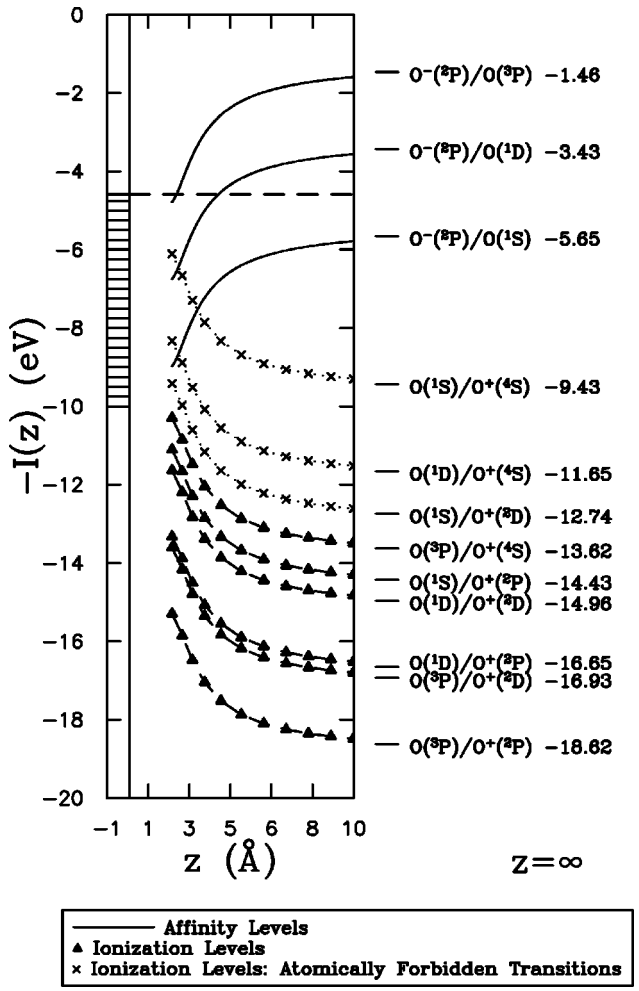

FIG. 6. Ionization and affinity levels I and A, respectively, of O near a Cu(001) surface. The levels included correspond to transitions between the states in Fig. 7. The zero of energy is the vacuum level, and the metal is in its lowest-energy state. The filled metal states are indicated by hatching. The asymptotic ionization and affinity energies for the isolated O atom are given on the right-hand side of the figure. Transitions allowed by spin and angular momentum conservation in the unperturbed atom are shown by dashed and solid lines, and prohibited transitions are shown with dotted lines. The latter are included because close to the surface the symmetry of the atom may be sufficiently perturbed that these transitions become possible. Due to the image potential the ionization levels shift up and the affinity levels shift down with decreasing z. The widths (not shown) of the levels increase roughly exponentially with decreasing z due to the hybridization of the atomic and metal states near the surface.

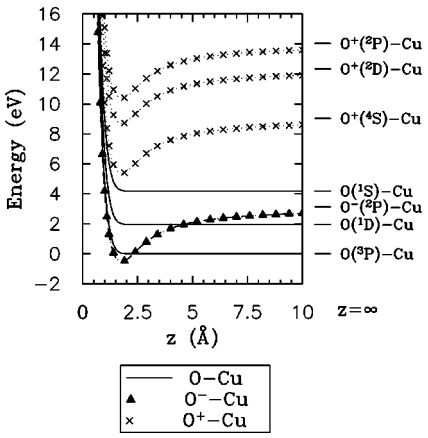

FIG. 7. The energies of the states of the O-Cu(001) system for which the metal is in its lowest-energy state (Ref. 37). The zero of energy is the energy of the O(^3P)-Cu state at $z=\infty$. The energies are plotted for clean Cu(001) with a work function of 4.59 eV. The energies of the O^+-Cu and O^--Cu states decrease with decreasing z due to the image potential, while the energies of the neutral states are taken to be constant. Close to the surface the energies of all the states increase due to the strongly repulsive interaction of the O and Cu electrons at small separations. The energy differences between states are determined by the work function of the surface ϕ and the ionization and affinity energies I and A for the corresponding oxygen levels (see Fig. 6). For example, the energy difference between the O^-(^2P)-Cu and O(^3P)-Cu states equals $(\phi - A_{O^-(^2P)/O(^3P)})$ at $z=\infty$; the ionization and affinity levels are labeled by the initial and final states involved. The energy difference decreases with decreasing z because of the attractive image potential.

Fermi level. Rather, it is determined by the simultaneous interaction of several atomic states with the metal. Furthermore, when several states need to be considered, the number of ionization and affinity levels increases rapidly. Below we use an equivalent description that relies simply on the energies of the states of the atom-surface system.[35]

Consider a set of basis states each of which consists of an atomic oxygen state and a metal state. We include the seven oxygen states presented above. The metal is characterized by its electron-hole pair excitations; the lowest-energy metal state has no electron-hole pairs, and the higher-energy states include all possible electron-hole pair combinations. We can divide these basis states into subspaces labeled by the atomic state. Figure 7 shows the lowest-energy state of each of these seven subspaces. Above each of these lowest-energy states is an infinite number of states that belong to that subspace, differing only by the excitation of the metal.[36,37] The energy of the lowest-energy O(^3P)-Cu state has been chosen to be zero at $z=\infty$, and the relative energies of the O-Cu states are determined by the usual arguments.[36,38,39]

In addition to their relative energies, we must also consider the couplings between the O-Cu states. For resonant charge-transfer processes, the important couplings are those for which the transfer of one electron takes the system from one state to another. In general, the manner in which the states in the O-Cu subspaces are coupled is complex;[36,39,40] however, here we need only consider that the couplings increase roughly exponentially with decreasing z, and so are largest close to the surface. This is equivalent in Fig. 6 to an exponential increase in the widths of the ionization and affinity levels with decreasing z, until a saturation width is reached. Very close to the surface widths are typically on the order of 1 eV.[18,41] The larger the couplings (widths) the greater the rate of electron transfer. Other types of couplings can also be important, for example, in Auger charge transfer, but we will not consider these explicitly here.

We consider first the resonant charge-transfer mechanism. The key principle is that the system will try to evolve toward the ground state of the O-Cu system by transferring electrons between the metal and the atom. The ground state along the outgoing trajectory[14,42] is a superposition of the O-Cu states, and since the relative energies and couplings of the states

change with separation, the contribution of each of these states to the ground state will also depend on the atom-surface separation. In general, the lower the energy of a state the larger its contribution to the ground state. The relevant energy scale is set by the strength of the coupling and corresponds to the width of the relevant affinity levels. From Fig. 7, we see that close to the surface the states that are separated from the lowest energy state by an amount less than or comparable to the width of the relevant affinity levels are the $O^-(^2P)$-Cu and $O(^3P)$-Cu states [and perhaps the $O(^1D)$-Cu states]. Far from the surface, where the couplings are small, the system is not strongly hybridized and the O-Cu system is in the lowest-energy $O(^3P)$-Cu state. The positive-ion states are always relatively high in energy and so constitute a very small part of the ground state at any distance from the surface.

There are two time scales in a scattering experiment that will influence the final charge-state probabilities. The first, set by the couplings between the states, determines the rate at a given distance from the surface at which the system evolves toward the ground state. The second, set by the velocity at which the atom leaves the surface and how the couplings and energies change with distance from the surface, determines how quickly the ground state changes along the outgoing trajectory. In a scattering experiment, if the outgoing perpendicular velocities are small enough, the system will equilibrate to the ground-state probabilities close to the surface and, as the atom leaves the surface, it will track the ground state by electron-transfer processes. At some separation, when the couplings are sufficiently small that the rate of charge transfer becomes smaller than the rate of change of the ground state, the system will lose track of the ground state (the charge transfer will become nonadiabatic), and the final charge-state distribution far from the surface will differ from the ground state.

Using the above arguments, it can be seen that both O^- and neutral O are expected in the scattered flux due to the resonant charge-transfer mechanism. The presence of O^+, however, cannot be explained in the same way. In Sec. IV C we propose an alternative mechanism that explains the observed O^+.

In addition to resonant charge transfer, we expect Auger charge transfer to be important in this system, particularly in neutralizing the positive ions on the incident trajectory. Rates for Auger processes are determined both by Auger couplings and by the number of electrons that are energetically accessible to participate in these processes. Since the oxygen ionization levels lie near the bottom of the Cu valence band, most electrons in the valence band are energetically available to participate in Auger processes. This is in contrast with alkali scattering where, since the ionization levels lie near the Fermi level, relatively few electrons are energetically allowed to take part in Auger processes.[39] Muller *et al.*[9] have shown that electrons, characteristic of Auger capture into the neutral oxygen ground state, are emitted when O^+ is scattered from clean W(110), providing further evidence that Auger processes must be considered. They also suggest that other kinds of Auger processes, such as Auger deexcitation, may have to be considered since electrons with energies characteristic of deexciting negative oxygen ions were observed when O^+ was scattered from cesiated W(110).

In conclusion, both Auger and resonant processes must be considered to describe the O-Cu system. In principle, with appropriate models and calculated couplings and energies, quantitative models could be used to determine the relative importance of these two mechanisms. Unfortunately, Auger rates for atoms near surfaces are poorly understood. Calculations of suitable couplings have only recently begun to appear in the literature,[7,8] and models are being developed that can simultaneously treat both resonant and Auger charge-exchange mechanisms.[39,43,44]

We turn now to a discussion of the data and what they tell us about charge-transfer mechanisms in the O-Cu system. In Secs. IV B and IV C we discuss the measured negative- and positive-ion yields separately.

B. Negative-ion formation

As discussed above, the negative ions in the scattered flux result from a nonadiabatic resonant charge-exchange mechanism. The O^- yields are expected to depend on the velocity of the scattered ions, with lower yields at lower perpendicular velocities. Although we have not measured absolute yields of scattered negative ions, Fig. 3 contains information about how the negative-ion yields vary with outgoing perpendicular velocity. We concluded in Sec. III A from the shape of the O^- angular spectra that the probability of scattering as a negative ion is relatively constant for energies above 2000 eV. However, for the 1000-eV and 400-eV O^- spectra, significant deviations from kinematic behavior are observed. In particular, the O^- intensities decrease with increasing final angle (decreasing perpendicular velocity). This implies that the probability that a negative ion will survive the outgoing trajectory decreases as the perpendicular velocity decreases; this is consistent with the system becoming more adiabatic at lower scattering velocities. Observations of O^- have previously been explained by several authors using resonant charge-transfer mechanisms.[3,5,18,20,45,46] Quantitative predictions of resonant charge-transfer probabilities require treating the intrinsic multistate character of this problem, including that arising from the degenerate *p* electrons in oxygen;[18] this is beyond the scope of this paper.

C. Positive-ion formation

Although we expect negative ions in the scattered flux due to nonadiabatic resonant charge exchange, as discussed above, this mechanism does not account for the scattered positive-ion yields. In this section, we will rule out various mechanisms for positive-ion production using arguments that are supported both by our data and by measurements performed by others. We then present the mechanism for positive-ion production that best explains the trends seen in our data.

An obvious source of positive ions is the incident beam. From our discussion above, we expect incoming positive ions to be efficiently neutralized either by Auger processes or by a combination of resonant and Auger processes. However, if the time spent in the near surface region is short enough, it is possible for an incident positive ion to scatter without being neutralized. That is, there may be memory of the incident charge state. However, we have recently repeated the measurements shown in Fig. 2 using incident O^-

beams. Within experimental uncertainties, the final O^+/O^- ratios are the same for incident O^- and O^+.[47] Beyond the obvious fact that a negative-ion beam cannot be the source of positive ions, this implies that there is loss of memory of the incident charge state and we must consider other mechanisms for the generation of positive ions. Similar conclusions have been reached in other studies; however, all of these studies have shown memory loss at much lower perpendicular velocities than our recent work. For example, for O^+ and O^- ions scattered from amorphous Si with incident energies as high as 19.9 keV, the ratio of O^+ to O^- ions in the scattered flux is independent of the incident charge state.[4] An important caveat to this is that the beam in this experiment was incident on the surface at a grazing angle, in which case the incident velocities perpendicular to the surface were equivalent to ions at normal incidence with energies no higher than 144 eV. Memory loss is not surprising at these low perpendicular velocities. Similar results have also been reported for scattering of multiply charged oxygen ions.[48] A recent report of scattering of O and O^- from Mg, Al, and Ag demonstrates memory loss for equivalent normal energies up to 424 eV.[5] In those experiments, O^+ is seen in the scattered flux when the incident species is O^- or O^0; once again, the scattered positive ions are not ions surviving from the incident beam. It is interesting to note, however, that in the scattering of noble gas atoms there are reports in which loss of memory of the incident charge state is not complete.[49] For example, in the scattering of 5-keV Ne^+ and Ne^0 from Cu(100),[49] the scattered positive ion fraction for incident Ne^0 was 1/30 that for incident Ne^+.

It is also possible for resonant charge exchange to produce positive ions. The strongly hybridized ground state of the O-Cu system close to the surface is an admixture of states. By the same arguments we used previously to discuss the negative-ion yields, there may be nonadiabatic survival of positive ions from the strongly hybridized state of the O-Cu system close to the surface.[36,38,40,50] We have argued above (Sec. IV A) that we expect the positive-ion yield resulting from this mechanism to be small because of the relatively high energies of the O^+-Cu states, but in the absence of quantitative calculations, we cannot rule this out as a mechanism of positive-ion production. Our experiments, however, provide evidence that an admixture of states due to proximity to the surface is not the primary source of scattered positive ions. As shown in Figs. 4 and 5, the broad background beneath the negative-ion QS peak is due to scattering from the deeper layers of the crystal. If we compare the positive- to negative-ion ratio of the background beneath the QS peak to that of the QS peak itself, we see that the background has a much smaller ratio. This is notable since both trajectories, the QS scattering and the deeper layer scattering, traverse the near-surface region at the same velocity. Hybridization near the surface should occur identically for the first and deeper layer trajectories causing their positive- to negative-ion ratios to be the same. This is clearly not consistent with the data.

It is also necessary to consider the effect of collision-induced perturbations of the surface. It has been shown previously that such perturbations can affect charge exchange via collision-induced changes in the electrostatic potential near the surface.[15] These changes can be modeled as a small shift in the Fermi energy (Fig. 6) or, equivalently, in the relative energies of the O-Cu states (Fig. 7). To determine if shifting the Fermi energy of the metal will significantly affect the final charge-state distribution we must compare the shift to the width of the atomic states. Very close to the surface the level widths are typically on the order of an eV; this is much larger than the few tenths of an eV shift induced by surface deformation, and, hence, the effect of the surface deformation on the final charge state will be small. Farther from the surface where the level widths are smaller, the same change in the surface potential can have a dramatic effect on the charge-state distribution.[15] Where we make this comparison, close to vs far from the surface, is determined by the final perpendicular velocity. At high velocities, the final charge state is determined close to the surface where the level widths are large. At lower velocities, the nonadiabatic determination of the final charge state occurs at some distance from the surface where the level widths are narrower. Since the final perpendicular velocities in our experiment are relatively high, the charge state is determined close to the surface where the level widths are large and, consequently, we do not expect collision-induced surface perturbations to be important.

Our data provide evidence that a hard collision with a surface copper atom is responsible for the scattered positive ions. To see this we begin by considering the ratio of scattered positive to negative ions shown in Fig. 2. As discussed in Sec. III B, the dramatic decrease in this ratio with decreasing perpendicular velocity is primarily due to a decrease in the positive-ion fraction. Two simple explanations can be given for this decrease. First, the slower the atom leaves the surface the more likely it is to suffer neutralization. Second, for a given scattering geometry, a lower perpendicular velocity corresponds to a lower incident energy and a less energetic collision. If the positive ions are generated in the collision, it is likely that a less energetic collision will give fewer positive ions.

To determine if the collision plays a role we look at the O^+/O^- ratio at a single perpendicular velocity for different geometries. For a given scattered perpendicular velocity, the O^+/O^- ratio is larger for a final angle of 65° than it is for a final angle of 45° (Fig. 2). In other words, the ratio does not simply scale with perpendicular velocity. For a given final perpendicular velocity, the ions with $\theta_f = 65°$ have lost approximately 1.7 times the energy lost by the ions with $\theta_f = 45°$; thus, for a given perpendicular velocity, the ions with $\theta_f = 65°$ have undergone a substantially more violent collision at the surface.

When comparing scattering at two different geometries, it is important to consider the difference in the velocity of the atom parallel to the surface. The effect of velocity parallel to the surface is to shift the Fermi surface of the metal in the rest frame of the atom.[17] This is similar in effect to a small change in the Fermi energy of the metal (Fig. 6) or to small changes in the relative energies of the O-Cu states (Fig. 7). As discussed above, small changes in these quantities are not important, indicating that the effect of parallel velocity will be negligible for the O-Cu system at keV energies.

Therefore, we conclude that the positive ions are generated primarily in QS collisions with first-layer atoms. In a QS collision, a 1–5-keV O^+ ion scattering through 70–90°

approaches within 0.3–0.6 Å of a single surface Cu atom. This is close enough to create core excitations in the scattered atom.[12,49] Because of the high scattered perpendicular velocities, the time spent near the surface is short enough that some memory of the charge-state distribution generated in the close collision can survive to affect the final scattered charge-state distribution. Although we have been able to determine that the positive ions are generated in the collision, we cannot determine the specific mechanism by which this occurs. One possibility is that the positive ions are generated by Auger autoionization of excited neutrals after they leave the surface. This process has recently been observed for a number of different systems.[5,10–13] Another possibility is that the collision introduces positive ions into the initial mix of states that gets propagated out from the surface and that some fraction of these survive.

V. SUMMARY

In summary, we have investigated the formation of O^+ and O^- ions that result from scattering of 0.4–7-keV O^+ from Cu(001). We use scattering geometries far from grazing for which trajectory analysis can be used to identify the scattered signal from specific trajectory types. In particular, we can distinguish quasisingle scattering trajectories from other types of trajectories. This has allowed us to identify a mechanism for positive-ion production, and to make quantitative measurements of the O^+/O^- ratio in the scattered flux for a single trajectory (collision) type.

From our data, from simple arguments based on the energies of the states of the O-Cu system, and from previous studies in the literature, we conclude that the scattered O^- ions result from a nonadiabatic resonant charge-exchange process. Other work in our group[47] indicates that the incident O^+ ions are neutralized on the incident trajectory by Auger processes, or by a combination of resonant and Auger processes.[3,9] We conclude that the positive ions observed in the scattered flux are generated in the hard collision of the incident atom with a surface Cu atom. Specifically, the shapes of the energy and angular spectra for scattered O^+ and O^-, and the dependence of the O^+/O^- ratio on scattering geometry, indicate that the positive ions observed in the scattered flux are generated in collisions with first-layer atoms.

ACKNOWLEDGMENTS

We thank Vladimir Esaulov, Jean-Pierre Gauyacq, Dominique Teillet-Billy, and especially Brad Marston, Eric Dahl, and Chad Sosolik for useful discussions. This research was supported by the National Science Foundation (Grants Nos. NSF-DMR-9313818 and NSF-DMR-9722771). Additional support was provided by the Air Force Office of Scientific Research (Grant No. AFOSR-91-0137). C.A.K. received primary support from the Fannie and John Hertz Foundation.

[1] H. Niehus, W. Heiland, and E. Taglauer, Surf. Sci. Rep. **17**, 21 (1993).

[2] A. Arnau, F. Aumayr, P. M. Echenique, M. Grether, W. Heiland, J. Limburg, R. Morgenstern, P. Roncin, S. Schippers, R. Schuch, N. Stolterfoht, P. Varga, T. J. M. Zouros, and H. P. Winter, Surf. Sci. Rep. **27**, 113 (1997).

[3] H. M. van Pinxteren, C. F. Avan Os, R. M. A. Heeren, R. Rodink, J. J. C. Geerlings, and J. Los, Europhys. Lett. **10**, 715 (1989).

[4] B. Hird, P. Gauthier, J. Bulicz, and R. A. Armstrong, Phys. Rev. Lett. **67**, 3575 (1991).

[5] M. Maazouz, V. A. Esaulov, L. Guillemot, T. Schlatholter, and S. Ustaze, Nucl. Instrum. Methods Phys. Res. B **215**, 283 (1997).

[6] R. Brako and D. M. Newns, Rep. Math. Phys. **52**, 655 (1989); J. Los and J. J. C. Geerlings, Phys. Rep. **190**, 133 (1990).

[7] T. Fonden and A. Zwartkruis, Phys. Rev. B **48**, 15 603 (1993).

[8] N. Lorente, R. Monreal, and M. Alducin, Phys. Rev. A **49**, 4716 (1994).

[9] H. Müller, G. Gador, H. Brenten, and V. Kempter, Surf. Sci. **313**, 188 (1994).

[10] K. A. H. German, C. B. Weare, and J. A. Yarmoff, Phys. Rev. Lett. **72**, 3899 (1994); Phys. Rev. B **50**, 14 452 (1994).

[11] O. Grizzi, M. Shi, H. Bu, J. W. Rabalais, and R. A. Baragiola, Phys. Rev. B **41**, 4789 (1990).

[12] T. M. Buck, W. E. Wallace, R. A. Baragiola, G. H. Wheatley, J. B. Rothman, R. J. Gorte, and J. G. Tittensor, Phys. Rev. B **48**, 774 (1993).

[13] L. Guillemot, S. Lacombe, V. A. Esaulov, and I. F. Urazgilden, Surf. Sci. **334**, 224 (1995).

[14] H. Brenten, H. Müller, A. Niehaus, and V. Kempter, Surf. Sci. **278**, 183 (1992).

[15] C. A. Keller, C. A. DiRubio, G. A. Kimmel, and B. H. Cooper, Phys. Rev. Lett. **75**, 1654 (1995).

[16] G. A. Kimmel and B. H. Cooper, Phys. Rev. B **48**, 12 164 (1993).

[17] J. N. M. van Wunnik, R. Brako, K. Makoshi, and D. M. Newns, Surf. Sci. **126**, 618 (1983); R. Zimny, H. Nienhaus, and H. Winter, Radiat. Eff. Defects Solids **109**, 9 (1989); R. Zimny, Surf. Sci. **233**, 333 (1990).

[18] B. Bahrim, D. Teillet-Billy, and J. P. Gauyacq, Surf. Sci. **316**, 189 (1994); Phys. Rev. B **50**, 7860 (1994).

[19] C. Auth, A. G. Borisov, and H. Winter, Phys. Rev. Lett. **75**, 2292 (1995).

[20] C. C. Hsu, H. Bu, A. Bousetta, J. W. Rabalais, and P. Nordlander, Phys. Rev. Lett. **69**, 188 (1992); C. C. Hsu, A. Bousetta, J. W. Rabalais, and P. Nordlander, Phys. Rev. B **47**, 2369 (1993).

[21] At keV energies, a quasisingle trajectory can be visualized as a simple two-body collision between the incident atom and a surface atom.

[22] M. Menzinger and L. Wåhlin, Rev. Sci. Instrum. **40**, 102 (1969).

[23] In addition to the ground state $(2p^3)O^+(^4S)$, there are two long-lived excited states $[2p^3(^2D)$ and $2p^3(^2P)]$ that are likely to be produced in our ion source. The $2p^3(^2D)$ state has an energy of 3.324 eV (Ref. 51) and a lifetime well over 10^3 s (Ref. 52). The $2p^3(^2P)$ state has an energy of 5.017 eV (Ref. 51) and a lifetime of 7.6 s (Ref. 51). Recent work in our group (Ref. 47) has shown that the final charge-state distribution does not depend on the incident beam.

[24] Galileo Electro-Optics Corp., Channeltron model 4830.

[25] G. A. Kimmel and B. H. Cooper, Rev. Sci. Instrum. **64**, 672 (1993).

[26] D. L. Adler and B. H. Cooper, Rev. Sci. Instrum. **59**, 137 (1988).

[27] R. L. McEachern, D. L. Adler, D. M. Goodstein, G. A. Kimmel, B. R. Litt, D. R. Peale, and B. H. Cooper, Rev. Sci. Instrum. **59**, 2560 (1988).

[28] The beam current measured on the sample during scattering is a function of sticking, secondary electron production, and charge exchange between the sample and scattering ions.

[29] C. A. Keller and B. H. Cooper, Rev. Sci. Instrum. **67**, 2760 (1996).

[30] E. R. Behringer, J. G. McLean, and B. H. Cooper, Phys. Rev. B **53**, 7510 (1996).

[31] This is not the case for the scattering geometry shown in Fig. 4 where the incident beam directly illuminates second layer atoms and produces QS-type trajectories, which cannot be distinguished from the QS trajectories that scatter from the first layer of atoms.

[32] Scattering geometries—and thus QS trajectories—are usually characterized by incident energy, incident angle, and final angle. When discussing charge exchange, it is often more convenient to think in terms of incident and final perpendicular velocities and the energy lost in the collision (i.e., collision energy). The collision energy corresponds to the distance of closest approach, but has the advantage of being independent of the atomic potentials. This set of parameters provides a natural separation into incident trajectory, collision, and final trajectory. $1/v_{\perp}$ for the scattered particles is proportional to the amount of time spent near the surface on the outgoing trajectory.

[33] D. M. Goodstein, S. A. Langer, and B. H. Cooper, J. Vac. Sci. Technol. A **6**, 703 (1988).

[34] J. P. Biersack and J. F. Ziegler, in *Ion Implantation Techniques*, edited by H. Ryssel and H. Glawischnig, Springer Series in Electrophysics Vol. 10 (Springer-Verlag, Berlin, 1982).

[35] Potential energy curves and how they relate to ionization and affinity level curves in the context of atom-surface charge transfer have been discussed previously in the literature. See, for example, N. D. Lang, J. K. Norskov, and B. I. Lundqvist, Phys. Scr. **34**, 77 (1986).

[36] E. B. Dahl, E. R. Behringer, D. R. Andersson, and B. H. Cooper, Int. J. Mass Spectrom. Ion Processes **174**, 267 (1998).

[37] In Fig. 7, there are an infinite number of states that sit above each state shown in the figure, forming a subspace of states. The lowest-energy state forms a lower bound for the subspace. The higher-energy states in the subspace correspond to excitations (e.g., electron-hole pairs) in the metal. As z varies, the energies of all the states in the subspace shift up or down by the same amount. Thus, to understand the relative energies of the states of the O-Cu system, it is sufficient to examine the energies of the lowest-energy states in the different subspaces. See, N. D. Lang and J. K. Norskov, Phys. Scr. **T6**, 15 (1983).

[38] J. B. Marston, D. R. Andersson, E. R. Behringer, B. H. Cooper, C. A. DiRubio, G. A. Kimmel, and C. Richardson, Phys. Rev. B **48**, 7809 (1993).

[39] A. V. Onufriev and J. B. Marston, Phys. Rev. B **53**, 13 340 (1996).

[40] E. B. Dahl and B. H. Cooper (unpublished).

[41] P. Nordlander, Phys. Rev. B **46**, 2584 (1992).

[42] We have assumed here that the incident trajectory is not important in determining the final electronic state since memory loss of the incident charge state is observed.

[43] A. T. Amos, B. L. Burrows, and S. G. Davison, Surf. Sci. Lett. **277**, L100 (1992); B. L. Burrows, A. T. Amos, Z. L. Miskovic, and S. G. Davison, Phys. Rev. B **51**, 1409 (1995).

[44] H. Müller, R. Hausmann, H. Brenten, A. Niehaus, and V. Kempter, Z. Phys. D **28**, 109 (1993).

[45] M. L. Yu, Phys. Rev. Lett. **47**, 1325 (1981).

[46] S. R. Kasi, M. A. Kilburn, Heon Kang, J. W. Rabalais, L. Tavernini, and P. Hochmann, J. Chem. Phys. **88**, 5902 (1988).

[47] A. Lavery, C. Sosolik, C. A. Keller, and B. H. Cooper (unpublished).

[48] L. Folkerts, S. Schippers, D. M. Zehner, and F. W. Meyer, Phys. Rev. Lett. **74**, 2204 (1995).

[49] S. B. Luitjens, A. J. Algra, E. P. Th. M. Suurmeijer, and A. L. Boers, Surf. Sci. **99**, 631 (1980).

[50] We have drawn a distinction between mixing with the band states close to the metal surface and mixing of atomic core states in a hard atom-atom collision that comes from the models used to treat charge exchange between atoms and surfaces. Resonant charge exchange models generally ignore the discrete atomic character of the surface and parametrize the interaction in terms of the atom surface separation z. In these models, at small z, there is a mixing of states that occurs independent of the lateral position of the scattering atom relative to the surface atoms. For metals, this treatment is easily justified by the delocalized character of the valance electrons. On the other hand, models for charge transfer between noble gases and surfaces generally focus on the interaction of localized core states. In this case, key parameters are the separations between the scattering atom and individual surface atoms. We must consider both of these when scattering keV O from Cu.

[51] A. A. Radzig and B. M. Smirnov, *Reference Data on Atoms, Molecules, and Ions*, Springer Series in Chemical Physics, Vol. 31 (Springer-Verlag, Berlin, 1985).

[52] W. L. Wiese, M. W. Smith, and B. M. Glennon, in *Atomic Transition Probabilities*, Natl. Bur. Stand. Ref. Data Ser., Natl. Bur. Stand. (U.S.) Circ. No. 4 (U.S. GPO, Washington, D.C., 1966), Vol. I.